

Theoretical review of various approaches in heavy quark production

Coordinators: M. Cacciari¹, E. Laenen²

Contributing authors: S.P. Baranov³, M. Cacciari¹, S. Diglio⁴, T.O. Eynck², H. Jung⁵, B.A. Kniehl⁶, S. Kretzer⁷, E. Laenen², A.V. Lipatov⁸, F. Maltoni⁹, F. Petrucci⁴, O.I. Piskounova³, I. Schienbein⁶, J. Smith^{2,10}, A. Tonazzo⁴, M. Verducci¹¹, N.P. Zotov⁸

¹LPTHE - Université P. et M. Curie (Paris 6), France

²NIKHEF Theory Group, Kruislaan 409, 1098 SJ Amsterdam, The Netherlands

³P.N. Lebedev Physical Institute of Russian Academy of Science, Moscow, Russia

⁴Università Roma Tre, Dipartimento di Fisica “E. Amaldi” and INFN Sezione Roma III, Via della Vasca Navale 84, 00146 Rome, Italy

⁵Deutsches Elektronen-Synchrotron Hamburg, FRG

⁶II. Institut für Theoretische Physik, Universität Hamburg, Luruper Chaussee 149, 22761, Hamburg, Germany

⁷ Brookhaven National Laboratory, Upton, NY 11973, USA

⁸D.V. Skobeltsyn Institute of Nuclear Physics, Moscow, Russia

⁹Institut de Physique Théorique, Université Catholique de Louvain, Chemin du Cyclotron, 2, B-1348, Louvain-la-Neuve, Belgium

¹⁰C.N. Yang Institute for Theoretical Physics, Stony Brook University, Stony Brook, NY 11794, USA

¹¹CERN, CH-1211 Genève 23, Switzerland

Abstract

We review some of the main theoretical aspects of heavy quark production at HERA that will be important for understanding similar processes at the LHC.

1 Introduction

The value for the LHC physics program of heavy quark production studies at HERA consists not only of measured quantities such as parton distributions, heavy quark masses etc. but at least as much of the theoretical ideas on heavy quark production that were developed and refined in the course of these studies. The strong experimental interest in heavy quark observables at HERA has led to a significantly increased understanding of the benefits and limitations of finite order calculations. It has stimulated theorists to deepen their insight into the issue of when a heavy quark should be treated as a parton, and it has provoked novel proposals to explain the hadronization of heavy quarks. In what follows we review and critically assess some of these ideas.

2 Heavy quark production

The study of heavy quarks, historically plagued by low production rates and large uncertainties, has now entered the regime of ‘precision physics’. On the one hand, the larger centre-of-mass energies of the colliders running now (Tevatron, HERA) and in the near future (LHC) lead to a much more copious production yield. On the other hand, technological advances such as the introduction of microvertex detectors based on semiconductor devices allow for much better tagging of the produced heavy flavours, and hence better measurements. Needless to say, an equally substantial improvement of the theoretical calculations has been needed in order to match this progress and therefore deliver predictions with an accuracy at least as good as that of the experimental measurements. Properly testing and constraining the theoretical calculations will in turn help in refining the predictions for the LHC.

One example for which a good theoretical accuracy at the LHC is desirable is in calculating the total Z boson production rate, a process which can be used as a luminosity candle and which we would like to have under control at the one per cent level. One channel contributing to this process is gluon-gluon fusion followed by bottom-antibottom annihilation, $gg \rightarrow b\bar{b} \rightarrow Z$. This channel provides about

5% of the total Z yield [1]: hence, it must be under control at the 20% level in order to achieve the sought-for final 1% accuracy.

As it turns out, it is more efficient and more reliable to rewrite this in terms of a perturbatively calculated parton distribution function (PDF) for the bottom quark, i.e. as the effective process $b\bar{b} \rightarrow Z$. The theoretical tools that we use to construct such heavy quark parton distribution functions must therefore be tested by employing them in other theoretical predictions, to be compared to the available experimental data. In the following section we shall list a number of examples where this is done.

From the point of view of ‘standard’ perturbative QCD calculations, the situation has not changed since the beginning of the ’90s: fully massive next-to-leading order (NLO) calculations were made available for hadron-hadron [2–6], photon-hadron [7–9] (i.e. photoproduction) and electron-hadron [10–13] (i.e. Deep Inelastic Scattering, DIS) collisions. These calculations still constitute the state of the art as far as fixed order results are concerned, and they form the basis for all modern phenomenological predictions.

Over the years, and with increasing experimental accuracies, it however became evident that perturbative QCD alone did not suffice. In fact, real particles - hadrons and leptons - are observed in the detectors, not the unphysical quarks and gluons of perturbative QCD. A proper comparison between theory and experiment requires that this gap be bridged by a description of the transition. Of course, the accuracy of such a description will reflect on the overall accuracy of the comparison. When the precision requirements were not too tight, one usually employed a Monte Carlo description to ‘correct’ the data, deconvoluting hadronization effects and extrapolating to the full phase space. The final ‘experimental’ result could then easily be compared to the perturbative calculation. This procedure has the inherent drawback of including the bias of our theoretical understanding (as implemented in the Monte Carlo) into an experimental measurement. This bias is of course likely to be more important when the correction to be performed is very large. It can sometimes become almost unacceptable, for instance when exclusive measurements are extrapolated by a factor of ten or so in order to produce an experimental result for a total photoproduction cross section or a heavy quark structure function.

The alternative approach is to present (multi)differential experimental measurements, with cuts as close as possible to the real ones, which is to say with as little theoretical correction/extrapolation as possible. The theoretical prediction must then be refined in order to compare with the real data that it must describe. This has two consequences. First, one has to deal with differential distributions which, in certain regions of phase space, display a bad convergence in perturbation theory. All-order resummations must then be performed in order to produce reliable predictions. Second, differential distributions of real hadrons depend unavoidably on some non-perturbative phenomenological inputs, fragmentation functions. Such inputs must be extracted from data and matched to the perturbative theory in a proper way, pretty much like parton distribution functions of light quarks and gluons are.

In the following sections we review the state of the art of theoretical calculations of heavy quark production in a number of high energy processes, pointing out similarities and differences. In particular, resummations aimed at improving the theoretical description of heavy quark production at large transverse momentum or large photon virtuality in DIS (Section 3), small centre-of-mass energy (Section 5) and large centre of-mass energy (Section 6) are described in some detail.

3 Collinear resummations and heavy quark PDFs

Perturbative calculations of heavy quark production contain badly converging logarithmic terms of quasi-collinear origin in higher orders when a second energy scale is present and it is much larger than the heavy quark mass m . Examples are the (square root of the) photon virtuality Q^2 in DIS and the transverse momentum p_T in either hadroproduction or photoproduction. Naming generically E the large scale, we

can write schematically the cross section for the production of the heavy quark Q as

$$\sigma_Q(E, m) = \sigma_0 \left(1 + \sum_{n=1} \alpha_s^n \sum_{k=0}^n c_{nk} \ln^k \left[\frac{E^2}{m^2} + \mathcal{O}\left(\frac{m}{E}\right) \right] \right), \quad (1)$$

where σ_0 stands for the Born cross section, and the coefficients c_{nk} can contain constants as well as functions of m and E , vanishing as powers of m/E when $E \gg m$.

Resummation approaches bear many different names, (ZM-VFNS, ACOT, FONLL, BSMN to name but a few) but they all share the goal of resumming leading ($\alpha_s^n \ln^n(E^2/m^2)$, LL) and sometimes also next-to-leading ($\alpha_s^n \ln^{n-1}(E^2/m^2)$, NLL) logarithmic terms to all orders in the cross section above. This is achieved by discarding power suppressed m/E terms, and factoring all the logarithms into a resummation factor, to be obtained via Altarelli-Parisi evolution of an initial condition set at the heavy quark mass scale,

$$\sigma_Q^{res}(E, m) = \sigma_0 C(E, \mu) f(\mu, m) = \sigma_0 C(E, \mu) E(\mu, \mu_0) f(\mu_0, m), \quad (2)$$

where μ and μ_0 represent artificial factorization scales, to be taken of order E and m respectively. The ‘products’ between the various functions actually hide convolution operations with respect to momentum fractions, not explicitly shown as arguments. $C(E, \mu)$ is a perturbatively calculable coefficient function, which does not contain large logarithms thanks to the choice $\mu \simeq E$. The function $f(\mu, m)$ can represent either a parton distribution or a fragmentation function for a heavy quark, and contains the resummation of the collinear logarithms. Due to the large heavy quark mass, its initial condition $f(\mu_0, m)$ can be calculated in perturbation theory [14, 15]: this is the distinctive feature that sets heavy quark parton and fragmentation functions apart from light flavour ones, whose initial conditions are instead entirely non-perturbative and must be fitted to data.

Once a massless but resummed result, valid in the $E \gg m$ region, is obtained, one would like to interpolate it with a fixed order cross section, valid instead in the $E \simeq m$ region, so as to retain predictivity over the whole E range.

The differences between the various approaches are then to be found essentially in two points:

- the perturbative order to which the initial condition $f(\mu_0, m)$ is evaluated, and the perturbative accuracy of the evolution;
- the way the matching with the fixed order calculation is performed.

We summarize below the features of the most commonly used implementations.

3.1 ACOT - Aivazis, Collins, Olness, Tung

This approach was the first to try to improve the prediction of the heavy quark structure functions $F_2^c(Q^2, m_c^2)$ and $F_2^b(Q^2, m_b^2)$ at large $Q^2 \gg m_c^2, m_b^2$, by moving potentially large logarithms $\ln(Q^2/m^2)$ into heavy quark parton densities [16, 17]. A general all-order analysis of factorization for the total inclusive $F_2(Q^2)$ in this context was presented in [18].

3.2 Simplified ACOT and ACOT(χ)¹

The original ACOT prescription [16, 17] has been simplified in [19] along lines suggested in [18, 20]. In a nutshell, diagrams with initial state heavy quark legs can be treated as if they represented massless quarks. More generally, the diagrams can be manipulated by power suppressed terms provided that higher order diagrams are regularized consistently. ACOT(χ) [21, 22] explores this freedom to improve on the threshold behaviour of partonic heavy quark schemes by enforcing the physical pair-production

¹Contributed by S. Kretzer

threshold on a term-by-term basis. Heuristically, it comes down to a simple re-scaling of Bjorken- x , i.e. in LO

$$F_2^{c\bar{c}} \propto c(\chi)|_{\chi=x_{\text{Bj}}(1+4m^2/Q^2)} \quad . \quad (3)$$

Physical arguments –mostly kinematic– have been given in [21–23], here we will establish the connection with the FONLL terminology of Section 1.3.3 while focusing on the inclusive DIS process. Much of the following has appeared before, in one form or another, in the literature [16–19, 24–28].

We formulate ACOT(χ) as an explicit manipulation of resummed terms of the perturbative series. We follow [24] in notation and add an $\mathcal{O}(\alpha_s^1)$ fixed order (FO) calculation to an all order collinearly resummed (RS) result. In RS heavy quark mass dependence other than logarithmic is neglected. When we remove double-counting terms from FO + RS the zero mass limit (FOM0) of the FO calculation will be required as an auxiliary quantity. Just as in RS, only asymptotic mass logarithms are retained in FOM0. We write therefore, as usual,

$$\sigma^{ACOT}(Q, m) = \text{FO} + (\text{RS} - \text{FOM0}) \times G \quad (4)$$

where G is an arbitrary operation which behaves like $G = 1 + \mathcal{O}\left(\frac{m^2}{Q^2}\right)$. In [24] G was chosen to be an overall multiplicative factor. More generally, it can be seen as an operation which only modifies, with $\mathcal{O}(m^2/Q^2)$ power-suppressed terms, perturbative coefficients beyond those which have been explicitly calculated, and which are therefore unknown anyway. Any choice for G with this behaviour is therefore legitimate.

To motivate the ACOT(χ) choice for G we first re-write more explicitly the three terms given above in the case of inclusive DIS:

$$\text{FO} = \alpha_s g \tilde{\otimes} H(Q, m) \quad (5)$$

$$\text{FOM0} = \alpha_s \left(g \otimes P_{qg}^{(0)} \ln \frac{\mu^2}{m^2} + g \otimes C_g \right) \quad (6)$$

$$\text{RS} = c(x) + \alpha_s (g \otimes C_g + c \otimes C_q) \quad (7)$$

where $H(Q, m)$ is the massive coefficient function for the FO gluon fusion process, C_g and C_q are the gluon and light quark coefficient functions (the $\overline{\text{MS}}$ scheme is implied), and g and c are the gluon and charm (i.e. heavy quark) parton distribution functions (both the coefficient functions and the PDFs depend, of course, on the factorization scale $\mu \simeq Q$). $P_{qg}^{(0)}$ is the leading order Altarelli-Parisi splitting vertex. The symbol $\tilde{\otimes} \equiv \int_{\chi}^1 d\xi/\xi \dots$ denotes a threshold-respecting convolution integral. One can convince oneself that the standard convolution \otimes , with $x \rightarrow \chi$ in the lower limit of integration, only differs by $\tilde{\otimes}$ by power-suppressed terms, $\tilde{\otimes} = \otimes + \mathcal{O}(m^2/Q^2)$.

The combined result (4) reads now

$$\begin{aligned} \sigma^{ACOT}(Q, m) &= \text{FO} + (\text{RS} - \text{FOM0}) \times G \\ &= \alpha_s g \tilde{\otimes} H + \left[c(x) - \alpha_s g \otimes P_{qg}^{(0)} \ln \frac{\mu^2}{m^2} + \alpha_s c \otimes C_q \right] \times G, \end{aligned} \quad (8)$$

and we recognize the Krämer-Olness-Soper simplified ACOT framework of [19]² if we set $G = 1$. Different choices for G can still be made, but natural demands are that:

- In kinematic regions where FO represents the relevant physics (i.e. $Q \sim m$), G should efficiently suppress uncontrolled spurious higher order terms in the square bracket of eq.(8).
- For computational efficiency, the simple $c(x)$ term alone should provide an optimized effective $\mathcal{O}(\alpha_s^0)$ approximation.

²See Eqs. (7), (8) there. General choices for G correspond to the discussion above these equations.

The ACOT(χ) scheme implements these requests by making an implicit choice for G which corresponds to writing

$$\begin{aligned}\sigma^{ACOT(\chi)}(Q, m) &= \text{FO} + (\text{RS} - \text{FOM0}) \times G \\ &= \alpha_s g \tilde{\otimes} H + \left[c(\chi) - \alpha_s g \tilde{\otimes} P_{qq}^{(0)} \ln \frac{\mu^2}{m^2} + \alpha_s c \tilde{\otimes} C_q \right].\end{aligned}\quad (9)$$

Further details on ACOT(χ) can be found in [21–23]. These articles also contain a more intuitive perspective of ACOT(χ). Moreover, [22] describes a PDF set that is consistent with ACOT(χ) applications.

3.3 BSMN - Buza, Smith, Matiounine, van Neerven

In Refs. [29–33] the treatment of heavy quarks as a parton was fully explored through next-to-next-leading order (NNLO), based on a precise two-loop analysis of the heavy quark structure functions from an operator point of view. This analysis yielded a number of results. One result is important beyond the observable at hand: the authors obtained the complete set of NNLO matching conditions for parton evolution across flavor thresholds. They found that, unlike at NLO, the matching conditions are *discontinuous* at the flavor thresholds. These conditions are necessary for any NNLO calculation at the LHC, and have already been implemented in a number of evolution packages [34, 35].

Furthermore, their two-loop calculations explicitly showed that the heavy *quark* structure functions in such a variable flavor approach are not infrared safe: one needs to either define a heavy *quark-jet* structure function, or introduce a fragmentation function to absorb the uncancelled divergence. In either case, a set of contributions to the inclusive light parton structure functions must be included at NNLO.

A dedicated analysis [36] for charm electroproduction showed that even at very large Q^2 one could not distinguish the fixed order NLO calculation of [10] and the NNLO VFNS calculations of [31], given the experimental data available in the year 2000. This demonstrates the possibility that the large logarithms $\ln(Q^2/m^2)$ together with small coefficients can in the end have little weight in the overall hadronic cross section.

3.4 FONLL - Fixed Order plus Next-to-Leading Log resummation

This approach was developed for improving the large- p_T differential cross section for heavy quark production in hadron-hadron collisions [37]. It was successively extended to photoproduction [38], and in a second phase a matching to the fixed order NLO calculations was performed [24, 39]. The FONLL acronym refers specifically to the matched version.

From the point of view of perturbative logarithms, it contains a NLO-accurate initial condition and full NLL evolution. It therefore reproduces the full NLL structure of the NLO calculation, and resums to all orders the large logarithms with NLL accuracy.

The matching with the fixed order result is performed according to the following master formula (see eq.(16) of [24]):

$$\sigma_Q^{\text{FONLL}}(p_T, m) = \text{FO} + (\text{RS} - \text{FOM0})G(m, p_T), \quad (10)$$

where FO stands for the NLO fixed order massive calculation, FOM0 for its $m/p_T \rightarrow 0$ limit (where however $\ln p_T/m$ terms and non-vanishing terms are kept), and RS for the massless, resummed calculation³. The RS–FOM0 subtraction is meant to cancel the terms which are present in both RS and FO. This difference starts therefore at order α_s^2 with respect to the Born cross section: at large p_T it resums

³This term might also be referred to as a ‘zero-mass variable flavour number scheme’ (ZM-VFNS) contribution. However this name, while by itself completely general, has been used in the past for specific approaches with different overall perturbative accuracies. We shall therefore avoid its use. It will be understood that ‘RS’ in this approach has full NLL accuracy.

correctly the NLL terms, at small p_T it only contains spurious terms, which are suppressed by the function $G(m, p_T) = p_T^2 / (p_T^2 + c^2 m^2)$, with $c = 5$, in order to ensure a physically correct behaviour. The choice of the suppression factor was motivated in [24] by the observation that the massless limit starts to approach the massive hadroproduction calculation at $\mathcal{O}(\alpha_s^3)$ only for $p_T > 5m$. Below this value the massless limit returns unreliable results, and its contribution must therefore be suppressed. It is important to realize that $G(m, p_T)$ only affects terms which are beyond the control of perturbation theory, and therefore it does not spoil the NLO+NLL accuracy. The choice to control such terms by means of an ad-hoc function might seem a somewhat unpleasant characteristic of this approach. However, it simply portrays the freedom one has in performing the matching, and does not represent a shortcoming of the approach: different matching procedures will simply make other implicit or explicit choices for $G(m, p_T)$.

For the sake of making comparisons with other approaches easier, the formula (10) can be rewritten with some more details as follows:

$$\begin{aligned} \sigma_Q^{\text{FONLL}}(p_T, m) &= \sum_{ij \in \mathcal{L}} F_i F_j \sigma_{ij \rightarrow QX}(p_T, m) \\ &+ \left(\sum_{ijk \in \mathcal{L} + \mathcal{H}} F_i F_j \hat{\sigma}_{ij \rightarrow kX}^{\overline{MS}}(p_T) D_{k \rightarrow Q} - \sum_{ij \in \mathcal{L}} F_i F_j \sigma_{ij \rightarrow QX}(p_T, m; m \rightarrow 0) \right) G(m, p_T) \end{aligned} \quad (11)$$

A few ingredients needing definition have been introduced. The kernel cross sections $\sigma_{ij \rightarrow QX}(p_T, m)$ are the massive NLO calculations for heavy quark production of Refs. [2–6]. When convoluted with the PDFs for light flavours F_i ($i \in \mathcal{L}$) they yield the FO term in eq. (10). The $\sigma_{ij \rightarrow QX}(p_T, m; m \rightarrow 0)$ terms represent the $m \rightarrow 0$ limit of the massive NLO cross sections, performed by sending to zero m/p_T terms while preserving $\ln(p_T/m)$ contributions and non-vanishing constants. When convoluted with light flavour PDFs they give FOM0. Finally, $\hat{\sigma}_{ij \rightarrow kX}^{\overline{MS}}(p_T)$ are the massless \overline{MS} -subtracted NLO cross section kernels given in [40]. In addition to the light flavour PDFs, they are also convoluted with the perturbatively-calculated parton distribution functions for the heavy quarks ($i \in \mathcal{H}$) and with the fragmentation functions describing the transformation of a parton into a heavy quark, $D_{k \rightarrow Q}$ [15], to give the term RS.

The formula given above returns the differential cross section for heavy *quark* production, evaluated with NLO + NLL accuracy. In order to obtain the corresponding cross section for an observable heavy meson it must still be convoluted with the proper scale-independent non-perturbative fragmentation function, extracted from experimental data, describing the heavy quark \rightarrow heavy hadron transition:

$$\sigma_H^{\text{FONLL}}(p_T, m) = \sigma_Q^{\text{FONLL}}(p_T, m) D_{Q \rightarrow H}^{NP} . \quad (12)$$

Phenomenological analyses of charm- and bottom-flavoured hadrons production within the FONLL approach have been given in [41–45].

3.5 GM-VFNS - General mass variable flavour number scheme

This approach also combines a massless resummed calculation with a massive fixed order one, for predicting p_T distributions in hadron-hadron collisions. One difference with respect to FONLL is that this approach does not include the perturbative NLO parton-to-heavy-quark fragmentation functions $D_{k \rightarrow Q}$. Rather, it directly convolutes a properly \overline{MS} subtracted cross section (with mass terms also included, hence the ‘general mass’ name) with non-perturbative fragmentation functions for heavy mesons $D_{Q \rightarrow H}^{NP, \overline{MS}}$, fitted at LEP in a pure \overline{MS} scheme. The cross section can be schematically written as

$$\sigma_H^{\text{GM-VFNS}}(p_T, m) = \sum_{ij \in \mathcal{L}} F_i F_j \hat{\sigma}_{ij \rightarrow QX}(p_T, m) D_{Q \rightarrow H}^{NP, \overline{MS}} + \sum_{ijk \in \mathcal{L} + \mathcal{H}} F_i F_j \hat{\sigma}_{ij \rightarrow kX}^{\overline{MS}}(p_T) D_{k \rightarrow H}^{NP, \overline{MS}} , \quad (13)$$

where the ‘massive-but-subtracted’ cross section kernels $\hat{\sigma}_{ij \rightarrow QX}(p_T, m)$ are defined by

$$\hat{\sigma}_{ij \rightarrow QX}(p_T, m) \equiv \sigma_{ij \rightarrow Q}(p_T, m) - \sigma_{ij \rightarrow QX}(p_T, m; m \rightarrow 0) + \hat{\sigma}_{ij \rightarrow QX}^{\overline{MS}}(p_T). \quad (14)$$

The new kernels $\hat{\sigma}_{ij \rightarrow QX}(p_T, m)$ defined by this operation (of the form FO-FOM0+RS) can be convoluted with an evolved \overline{MS} -subtracted fragmentation function, but they also retain power suppressed m/p_T terms. It should also be noted that the sum in the second term of (13) only runs over contributions not already included in the first.

Recalling the way the perturbative parton-to-heavy-quark $D_{k \rightarrow Q}$ fragmentation functions are defined in [15], setting

$$D_{k \rightarrow H}^{NP, \overline{MS}} = D_{k \rightarrow Q} D_{Q \rightarrow H}^{NP}, \quad k \in \mathcal{L} + \mathcal{H}, \quad (15)$$

and comparing eqs.(13) and (11), it can be seen that the GM-VFNS master formula is a reshuffling of the FONLL one, up to higher-orders terms.

Two comments are worth making. The first is that due to the absence of the perturbative $D_{k \rightarrow Q}$ terms, eq. (13) cannot reproduce the NLO heavy *quark* production cross section: even the normalization must be extracted from the experimental data. Eq. (11), on the other hand, can reproduce the heavy quark spectrum, and only the heavy quark \rightarrow heavy meson transition is fitted to data. The second remark concerns the higher order power suppressed terms: since GM-VNFS implicitly makes a different choice for the $G(m, p_T)$ function, the results from the two approaches might differ considerably in the $p_T \sim m$ region since, while formally suppressed, such terms can be numerically important.

An example of a phenomenological application of the GM-VFNS scheme is given below.

3.6 Hadroproduction of heavy mesons in a massive VFNS⁴

Various approaches for next-to-leading-order (NLO) calculations in perturbative QCD have been applied to one-particle-inclusive hadroproduction of heavy mesons. The general-mass variable-flavor-number scheme (GM-VFNS) devised by us in Ref. [46, 47] is closely related to the conventional massless variable-flavor-number scheme (ZM-VFNS), but keeps all m^2/p_T^2 terms in the hard-scattering cross sections, where m is the mass of the heavy quark and p_T the transverse momentum of the observed meson, in order to achieve better accuracy in the intermediate region $p_T \geq m$. The massive hard-scattering cross sections have been constructed in such a way that the conventional hard-scattering cross sections in the \overline{MS} scheme are recovered in the limit $p_T \rightarrow \infty$ (or $m \rightarrow 0$). The requirement to adjust the massive theory to the ZM-VFNS with \overline{MS} subtraction is necessary, since all commonly used PDFs and FFs for heavy flavors are defined in this particular scheme. In this sense, this subtraction scheme is a consistent extension of the conventional ZM-VFNS for including charm-quark mass effects. It should be noted that our implementation of a GM-VFNS is similar to the ACOT scheme [16, 17], which has been extended to one-particle-inclusive production of B mesons a few years ago [48]. As explained in the second paper of Ref. [46, 47], there are small differences concerning the collinear subtraction terms. Furthermore, in Ref. [48], the resummation of the final-state collinear logarithms has been performed only to leading logarithmic accuracy. The field-theoretical foundation of a GM-VFNS has been provided a few years ago by a factorization proof including heavy-quark masses [18]. Therefore, it is possible to extract improved universal parton distribution functions (PDFs) [22] and fragmentation functions (FFs) [49] from fits employing massive hard-scattering cross sections. From this perspective, it is important to compute massive hard-scattering cross sections in a given massive scheme for all relevant processes. Explicit calculations in the original ACOT scheme have been performed in Ref. [50, 51] for inclusive and semi-inclusive deep-inelastic scattering (DIS). Furthermore, our calculation in Ref. [46, 47] for hadronic collisions completes earlier work in the GM-VFNS on D -meson production in $\gamma\gamma$ and γp collisions [52–54], and it is planned to extend our analysis to the case of heavy-meson production in DIS.

⁴Contributed by B.A. Kniehl and I. Schienbein.

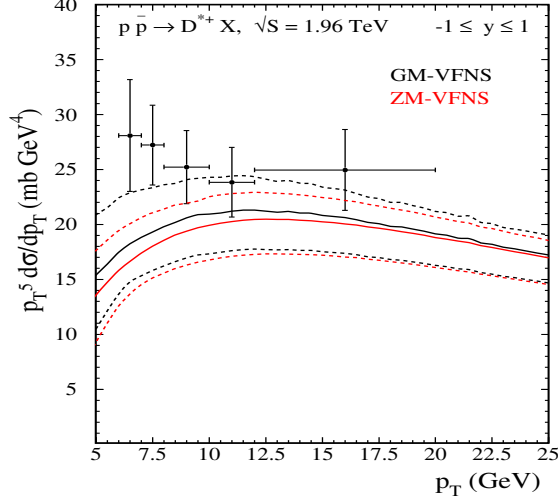


Fig. 1: QCD predictions for one-particle-inclusive production of D^* mesons at the Tevatron Run II in comparison with CDF data [57]. The results are shown for the average $D^* = (D^{*+} + D^{*-})/2$. The solid lines have been obtained with $\mu_R = \mu_F = \mu'_F = m_T$. The upper and lower dashed curves represent the maximum and minimum cross sections found by varying μ_R , μ_F , and μ'_F independently within a factor of 2 up and down relative to the central values while keeping their ratios in the range $0.5 \leq \mu_F/\mu_R, \mu'_F/\mu_R, \mu_F/\mu'_F \leq 2$.

Next, we show predictions for the cross section $d\sigma/dp_T$ of D^* -meson production obtained in the GM-VFNS and the ZM-VFNS. The cross section has been scaled with p_T^5 in order to arrive at a flat p_T distribution, which is useful for visualizing the heavy-quark mass effects. The hard-scattering cross sections are convoluted with the (anti-)proton PDFs and FFs for the transition of the final-state parton into the observed D^* meson. We use the CTEQ6M PDFs [55] and the FFs for D^* mesons from Ref. [56]. As in the experimental analysis, the theoretical results are presented for the average $(D^{*+} + D^{*-})/2$. We consider $d\sigma/dp_T$ at $\sqrt{S} = 1.96$ TeV as a function of p_T with y integrated over the range $-1.0 < y < 1.0$. We take the charm mass to be $m = 1.5$ GeV and evaluate $\alpha_s^{(n_f)}(\mu_R)$ with $n_f = 4$ and scale parameter $\Lambda_{\overline{MS}}^{(4)} = 328$ MeV, corresponding to $\alpha_s^{(5)}(m_Z) = 0.1181$. The results are presented in Fig. 1 for the GM-VFNS (black lines) and the ZM-VFNS (red lines) in comparison with CDF data [57]. The solid lines have been obtained with $\mu_R = \mu_F = \mu'_F = m_T$. The upper and lower dashed curves represent the maximum and minimum cross sections found by varying μ_R , μ_F , and μ'_F independently within a factor of 2 up and down relative to the central values requiring for their ratios to satisfy the inequalities $0.5 \leq \mu_F/\mu_R, \mu'_F/\mu_R, \mu_F/\mu'_F \leq 2$. As can be seen, for large values of p_T , the predictions of the GM-VFNS nicely converge to the corresponding results in the ZM-VFNS. Both approaches lead to reasonable descriptions of the data, but the inclusion of the positive mass effects clearly improves the agreement with the data. It should be noted that the mass effects are largest for the upper curves of the uncertainty band, which have been obtained with the smaller value of the renormalization scale implying a larger $\alpha_s(\mu_R)$. At $p_T = 5$ GeV, one observes an increase of the massless cross section by about 35%. A more detailed comparison of the GM-VFNS with CDF data [57] including D^0 , D^+ , and D_s^+ mesons can be found in Refs. [58, 59].

Residual sources of theoretical uncertainty include the variations of the charm mass and the employed PDF and FF sets. A variation of the value of the charm mass does not contribute much to the theoretical uncertainty. Also, the use of other up-to-date NLO proton PDF sets produces only minor differences. Concerning the choice of the NLO FF sets, we obtain results reduced by a factor of 1.2–1.3 when we use the NLO sets from Ref. [60], which is mainly caused by a considerably different gluon FF. A more detailed discussion can be found in Ref. [56].

Table 1: Process relevant for SM measurements and SUSY discoveries at the LHC which entail the use of bottom in the initial state. All of them are known at least at NLO accuracy.

Name	LO Process	Interest	Accuracy
single-top t-channel	$qb \rightarrow qt$	top EW couplings	NLO
single-top tW-associated	$gb \rightarrow tW^-$	Higgs bckg, top EW couplings	NLO
Vector boson + 1 b-jet	$gb \rightarrow (\gamma, Z)b$	b-pdf, SUSY Higgs benchmark	NLO
Vector boson + 1 b-jet +1 jet	$qb \rightarrow (\gamma, Z, W)bq$	single-top and Higgs bckgs	NLO
Higgs inclusive	$b\bar{b} \rightarrow (h, H, A)$	SUSY Higgs discovery at large $\tan \beta$	NNLO
Higgs + 1 b-jet	$gb \rightarrow (h, H, A)b$	SUSY Higgs discovery at large $\tan \beta$	NLO
Charged Higgs	$gb \rightarrow tH^-$	SUSY Higgs discovery	NLO

4 A case study in collinear resummation: b -quark PDF from $Z + b$ production at LHC⁵

4.1 Introduction

The discovery of new physics at LHC will probably rely on the detailed understanding of standard-model background processes. Outstanding among these is the production of weak bosons (W, Z) in association with jets, one or more of which contains a heavy quark ($Q = c, b$). The prime example is the discovery of the top quark at the Fermilab Tevatron, which required a thorough understanding of the W +jets background, with one or more heavy-quark jets. The discovery of single-top-quark production via the weak interaction will require an even more sophisticated understanding of this background [61, 62].

For many processes involving production of heavy quarks, there are two ways (schemes) to perform the calculation in QCD: the fixed-flavor-scheme (FFS) and variable-flavor-scheme (VFS). The main practical difference between the two approaches is simple: in the VFS the heavy-quark can also be in the initial state, and in that case is assumed to be massless, while in the FFS it appears only as a final state (massive) particle. QCD factorisation tells us that if calculations could be performed at arbitrary high order, the two schemes would be equivalent. At fixed order, on the other hand, differences arise and one should choose that describing more effectively the kinematics of the process of interest. This freedom has sometimes created intense and fruitful debates among the QCD practitioners (see, *e.g.*, Ref. [63] for a detailed comparison of Higgs boson production in association with bottom quarks). Here we just recall the main two reasons for using a heavy-quark distribution function. First, it resums collinear logarithms of the form $\ln Q/m_Q$ to all orders, where Q is the scale of the hard scattering and m_Q is the mass of the heavy quark. Second, it simplifies the leading-order process, which often makes a higher-order calculation feasible. There are many processes in the standard model and in models beyond it, such as SUSY, that are better described using a bottom in the initial state. In Table 1, we give a non-exhaustive list of processes that will be relevant for QCD, EW and SUSY studies at the LHC, and the QCD order at which they are known.

At present the b distribution function is derived perturbatively from the gluon distribution function [17, 18, 34, 55]. Recently, direct, albeit not very precise, measurements of F_2^b have become available that are compatible with the perturbative determination [64, 65]. In the light of its phenomenological importance, a better direct determination of the b distribution function is certainly desirable.

To this aim it has been proposed to use the associated production of a photon and a b -jet via $gb \rightarrow \gamma b$ at the LHC [66]. This measurement suffers from two main limitations. The first is the large contamination from charm which has a much larger cross section due to both the pdf and the electromag-

⁵Contributed by S. Diglio, F. Maltoni, F. Petrucci, A. Tonazzo and M. Verducci

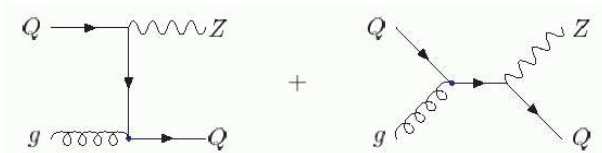


Fig. 2: Leading Order Feynman diagrams for associated production of a Z boson and a single high- p_T heavy quark ($Q = c, b$).

netic coupling. The second is that the theoretical prediction at NLO for an isolated photon is uncertain, due to necessity of introducing a photon fragmentation function, which is at present poorly known.

In this note we follow the suggestion of Ref. [67] to use Z production in association with a b -jet to extract information on the b -pdf. At leading order, it proceeds via $gb \rightarrow Zb$, as shown in Fig. 2. This process is known at NLO, including γ/Z interference effects. The advantages of using a γ/Z decaying into leptons with respect to a real photon are noticeable. The NLO cross section is theoretically very well known and, apart from the PDF's, free of non-perturbative inputs. In addition, the competing process $gc \rightarrow Zc$ is suppressed by the ratio of the couplings of the charm and the bottom to the Z , and makes the b -pdf determination much cleaner.

The D0 Experiment at Tevatron has recently measured the cross-section ratio $\sigma(Z + b)/\sigma(Z + jet)$ [68], and their result is consistent with the NLO calculation.

As pointed out in [67], the measurement of this process at the LHC should be even more interesting because the contribution of the leading order process, sensitive to the b content of the proton, is more relevant than at the Tevatron. In addition, the total cross-section is larger by a factor 50, and the relative contribution of background processes, mainly $Z+c$, is smaller. These features are summarised in Table 2, taken from Ref. [67].

Table 2: Next-to-leading-order inclusive cross sections (pb) for Z -boson production in association with heavy-quark jets at the Tevatron ($\sqrt{s} = 1.96$ TeV $p\bar{p}$) and the LHC ($\sqrt{s} = 14$ TeV pp). A jet lies in the range $p_T > 15$ GeV/c and $|\eta| < 2$ (Tevatron) or $|\eta| < 2.5$ (LHC). ZQ indicates events containing a heavy quark, Zj events which do not contain a heavy quark.

Cross sections (pb)	Tevatron	LHC
Process	ZQ inclusive	
$gb \rightarrow Zb$	$13.4 \pm 0.9 \pm 0.8 \pm 0.8$	$1040^{+70+70}_{-60-100} \text{ }^{+30}_{-50}$
$gb \rightarrow Zb\bar{b}$	6.83	49.2
$gc \rightarrow Zc$	$20.3^{+1.8}_{-1.5} \pm 0.1^{+1.3}_{-1.2}$	$1390 \pm 100^{+60+40}_{-70-80}$
$gc \rightarrow Zc\bar{c}$	13.8	89.7
	Zj inclusive	
$q\bar{q} \rightarrow Zg, gq \rightarrow Zq$	$1010^{+44+9+7}_{-40-2-12}$	$15870^{+900+60}_{-600-300} \text{ }^{+300}_{-500}$

Besides the possibility of extracting the b -pdf, $Z + b$ represents also a benchmark and in some cases a background to the search of the Higgs boson, when it is produced in association with a single high- p_T b quark [63]: the dominant leading-order subprocess for the production of a Higgs boson via its coupling to the b is $b\bar{b} \rightarrow h$; however, if the presence of a single b with high p_T is demanded, the dominant process becomes $gb \rightarrow hb$, with cross-sections of the order of tens of fb. The h can then decay to the same final states as the Z ; in particular, the decay $h \rightarrow \mu^+\mu^-$ is enhanced in some models [69–71].

A preliminary analysis on the potential of the ATLAS experiment to measure the $Z+b$ -jet production at the LHC is presented in the following.

4.2 A study of LHC measurement potential

A sample of Z +jet events generated using the PYTHIA Monte Carlo [72] was processed with a fast simulation of the ATLAS detector, the ATLFast package [73]. Only decays of the Z boson to $\mu^+\mu^-$ were taken into account. The signal was defined as the sample events containing a b quark with $p_T > 15$ GeV/ c and $|\eta| < 2.5$. The background samples containing respectively a c quark within the same cuts, or a jet originating from a light quark or a gluon in the same range, were considered separately. The NLO cross-sections computed in [67] were used for the signal and for these two classes of background, while the cross-section given by PYTHIA was taken for the other types of events.

The experimental selection of Z +jet events with $Z \rightarrow \mu^+\mu^-$ required the detection of two muons of opposite charge with $p_T > 20$ GeV/ c and $|\eta| < 2.5$ and one hadronic jet. The presence of two high- p_T muons ensures the possibility to have high trigger efficiency on this type of events. In addition, to reject the contribution from virtual photons, the invariant mass $M_{\mu\mu}$ of the muon pair was required to be close to the Z mass ($80 \text{ GeV}/c^2 < M_{\mu\mu} < 105 \text{ GeV}/c^2$). About 50% of signal events are retained after applying these cuts, the loss being equally due to the η acceptance and to the p_T cut.

The selection of events where the jet originates from a b quark was based on two different tagging methods, as described in the following. Their complementarity is still to be studied in detail, however the comparison of two independent selections will be important to control the systematic uncertainties.

The first method to select $Z + b$ events was based solely on the presence of a third muon. Hadrons containing a b quark give origin to prompt muon decays in about 12% of the cases. The efficiency of this method, therefore, cannot exceed this value, however the background is also expected to be small. The ‘‘third muon’’, considered to be the muon from the b hadron decay, will in general be softer and closer to a jet than the muons from the Z decay. The distribution of the transverse momentum of the third muon in $Z + j$ events is shown in Fig. 3. Different thresholds on the third muon p_T were considered for the final selection.

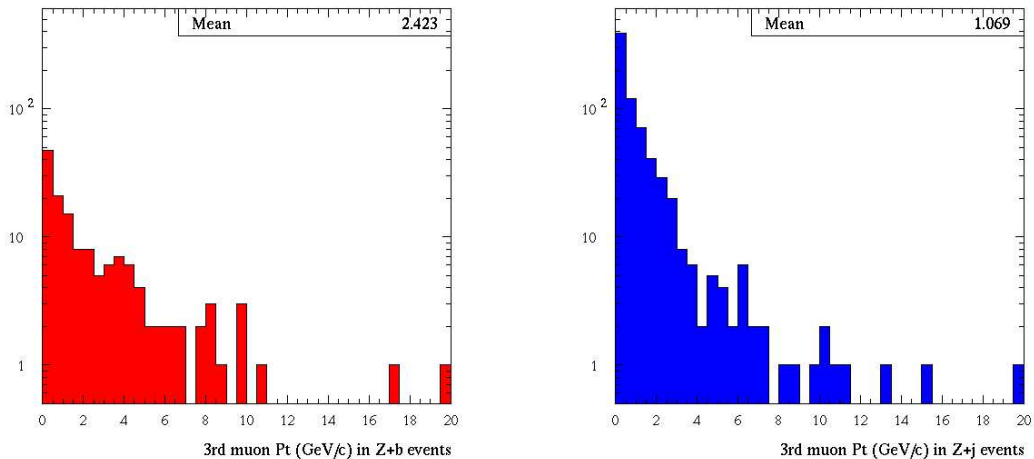


Fig. 3: Distribution of the transverse momentum of the third muon in a Z +jet sample, for signal events (left) and for events with no b quark (right).

The second analysis used an inclusive method for b -tagging, based on the presence of secondary vertices and of tracks with high impact parameter with respect to the primary vertex, originated from the

Table 3: Expected efficiency, statistics and purity in a data sample corresponding to an integrated luminosity of 10 fb^{-1} , using the soft muon tagging with different thresholds on the muon transverse momentum and the inclusive b -tagging. N_b denotes the number of expected signal events as defined in the text, N_c the number of selected events with a c jet with $p_T > 15 \text{ GeV}$ and $|\eta| < 2.5$, N_{other} the selected events from other processes. The statistical error on efficiencies and purities, due to the limited size of the simulated sample, is at the level of 1-2%.

Cut	Efficiency	$N_b^{p_T > 15 \text{ GeV}, \eta \leq 2.5}$	$N_c^{p_T > 15 \text{ GeV}, \eta \leq 2.5}$	N_{other}	Purity
$p_T^\mu > 4 \text{ GeV}/c$	4%	13990	6270	0	69%
$p_T^\mu > 5 \text{ GeV}/c$	3%	11090	5210	0	69%
$p_T^\mu > 6 \text{ GeV}/c$	2.5%	8430	4180	0	67%
incl. b -tag	14%	49500	17400	49600	43%

decay of the long-lived b hadrons. The ATLFASST package reproduces the ATLAS b -tagging capabilities by applying the tagging efficiency on b jets and a mis-tag rate on non- b jets on a statistical basis, according to the values set by the user to reproduce the actual detector performance. The efficiency of the inclusive b -tagging on signal events, after the selection described above, is about 30%. The mistagging probability is about 4% on c -quark jets and 0.5% on light jets.

The overall efficiency on signal events, the expected number of signal and background events with an integrated luminosity of 10 fb^{-1} and the expected purity of the selected samples are reported in table 3. With the fast simulation, the soft muon tagging capabilities are optimistic, in that full efficiency and no mis-tag are assumed for the lepton identification; more realistic assumptions will be made when the study is carried on with the full detector simulation. The efficiency on signal events achieved with the inclusive b -tagging method, where the results of the fast simulation are more realistic, is higher than with the soft muon tagging, while the purity of the selected sample is still quite good. Consistent results were obtained with a full simulation of the ATLAS experiment, on a small statistics sample.

A better determination of the signal component in the selected sample will eventually be achieved by exploiting the information on the transverse momentum of the b -jet or of the third muon.

Given the large statistics of the available data samples, the measurement will be limited by systematic effects.

The possibility to control the systematic effects directly from data samples has been explored, in particular the evaluation of b -tagging performance and of the residual background.

The b -tagging efficiency can be checked using b -enriched samples. Based on previous experience at Tevatron and LEP, we can expect a relative uncertainty of about 5%.

The background in the selected sample is mainly due to mis-tagged jets from c and light quarks. This can be controlled by looking at the number of b -tagged jets in data samples that in principle should contain no b -jets at first order. W +jet events, for example, will be available with large statistics and with jets covering the full p_T range of the signal. It can therefore be expected to estimate the background from mis-tagging with a relative uncertainty at the level of few percent, as shown by the plots in figure 4.

4.3 Conclusions and outlook

Z boson production in association with a b -jet can provide information on the b -pdf.

A preliminary study of the $Z + b$ channel using a fast simulation of the ATLAS detector has shown that this type of event will be observed with very high statistics and good purity at the LHC. Given the large statistics of the samples, the precision of the $Z + b$ cross-section measurement will be limited by systematic effects. Some possibilities to evaluate systematic uncertainties directly from the data have

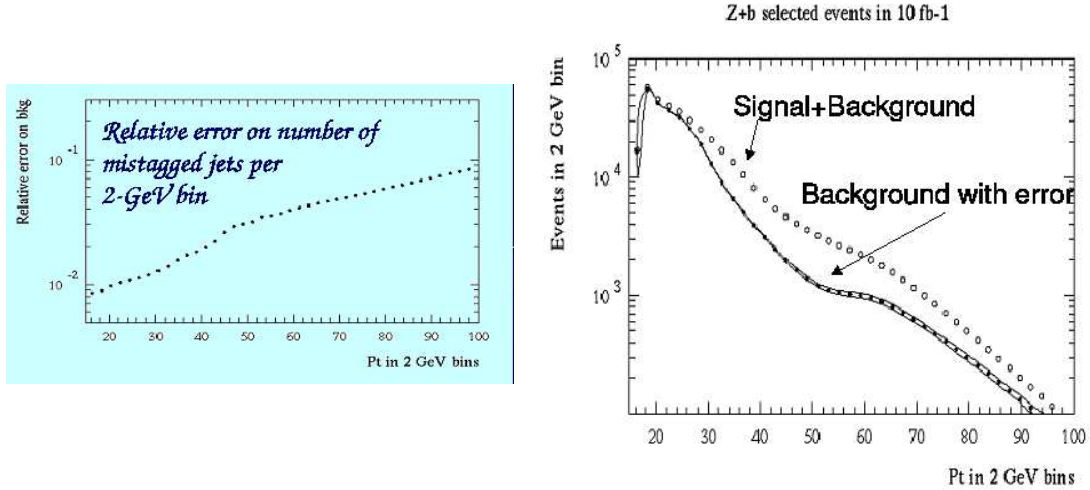


Fig. 4: Systematics due to mis-tagging of b -jets as evaluated from W +jet events. Left: relative error on background level per jet p_T bin. Right: p_T distribution of jets in event selected as $Z + b$; the error band on the background contribution represents the systematic uncertainty, as derived from the previous plot.

been considered. An overall accuracy on the measurement at the level of 5% can be expected.

The availability of large samples opens interesting possibilities for the study of differential distributions: for instance, measuring the cross-section as a function of the η and p_T of the Z boson would allow for the measurement of the b PDF as a function of the momentum fraction carried by the quark inside the proton. These items are an additional topic for further studies.

5 Soft-gluon resummation⁶

QCD factorizes long- and short distance dynamics in inclusive cross sections with initial state hadrons into non-perturbative, but universal parton distribution functions, and perturbatively calculable hard scattering functions. Large remnants of the long-distance dynamics occur near the threshold edge of phase space in the form of logarithmic distributions that are singular at the edge. Resummation [74,75] of these effects organizes them to all orders in perturbation theory, and thereby extends the predictive power of QCD.

Threshold resummation is now a well-established calculational scheme with systematically improvable accuracy. It allows organization of all subleading powers of the logarithmic enhancements, and can be consistently matched to finite order perturbation theory. Resummed expressions, which take the form of exponentiated integrals over functions of the running coupling, require however a prescription for their numerical evaluation to handle a Landau pole singularity of the coupling. But for this intrinsic ambiguity (which must cancel against ambiguities in power corrections), threshold resummation is just as systematically improvable as the standard coupling constant expansion.

As stated earlier, the more differential a cross section, the better suited it is for phenomenology, because one may incorporate detector-specific acceptance cuts and thereby reduce the need for extrapolation. Therefore we should like to better understand the behavior of threshold-resummed expressions for double-differential cross sections. A study for the inclusive threshold-resummed heavy quark structure function can be found in Ref. [76]. Here we examine the differential structure function for the reaction

$$\gamma^*(q) + P(p) \rightarrow Q(p_1) + X'(p'_2) \quad (16)$$

⁶Contributed by T.O. Eynck and E. Laenen.

which we write as

$$\frac{d^2 F_2^Q(S, T_1, U_1)}{dT_1 dU_1} \quad (17)$$

We define the invariants

$$\begin{aligned} S &= (p+q)^2 \equiv S' - Q^2, & T_1 &= (p-p_1)^2 - m^2, \\ U_1 &= (q-p_1)^2 - m^2, & S_4 &= S' + T_1 + U_1. \end{aligned} \quad (18)$$

The invariant mass squared of the final state X' is given by

$$M_{X'}^2 = m^2 + S_4 \quad (19)$$

so that the elastic (threshold) limit for the subprocess (16) is approached by $S_4 \rightarrow 0$. It may be converted to the double-differential structure function in terms of the heavy quark transverse momentum and rapidity, e.g.

$$\frac{d^2 F_k^Q}{d(p_T^Q)^2 dy^Q} = S' \frac{d^2 F_k^Q}{dT_1 dU_1}, \quad (20)$$

where e.g. [11]

$$p_T^Q = \left[\frac{S' T_1 U_1 + Q^2 T_1^2 + Q^2 S' T_1}{S'^2} - m^2 \right]^{(1/2)}. \quad (21)$$

At the parton level one may define invariants equivalent to those in (18), which we will denote by using lower case. The order-by-order perturbation theory expansion for the partonic version of this distribution $\omega(s_4, t_1, u_1)$ and its all-order resummation have the following schematic forms

$$\begin{aligned} \omega &= 1 + \alpha_s(L^2 + L + 1) + \alpha_s^2(L^4 + L^3 + L^2 + L + 1) + \dots \\ &= \exp \left(\underbrace{\underbrace{L g_1(\alpha_s L) + g_2(\alpha_s L) + \dots}_{LL}}_{NLL} \right) \underbrace{C(\alpha_s)}_{\text{constants}} \\ &\quad + \text{suppressed terms} \end{aligned} \quad (22)$$

with

$$g_1(\lambda) = \frac{C_F}{\pi b_0 \lambda} \left[\lambda + (1 - \lambda) \ln(1 - \lambda) \right], \quad \lambda = b_0 \alpha_s \ln N. \quad (23)$$

(We have also computed $g_2(\lambda)$; by including ever more g_i functions in the exponent in Eq. (22) we can increase the parametric accuracy of the resummation.) The symbol L^i represents, in this case, the logarithmically singular plus-distributions

$$\left[\frac{\ln^{i-1}(\rho)}{\rho} \right]_+ \quad (24)$$

with $\rho = s_4/m^2$, or, after a Laplace transform $\int d\rho \exp(-N\rho)$ by $\ln^i N$. The conversion to momentum space then requires a numerical inverse Laplace transform. For the case at hand one needs to compute

$$S'^2 \frac{d^2 F_2^Q(S_4, T_1, U_1)}{dT_1 dU_1} = \int_{c-i\infty}^{c+i\infty} \frac{dN}{2\pi i} e^{NS_4/m^2} \bar{\phi}_g \left(N \frac{S' + T_1}{m^2} \right) \omega(N, T_1, U_1), \quad (25)$$

with c the intercept of the contour with the real N axis, and $\phi_g(N)$ the gluon density in moment space. We chose a toy density for the gluon PDF, and the minimal prescription [77] to perform the N integral.

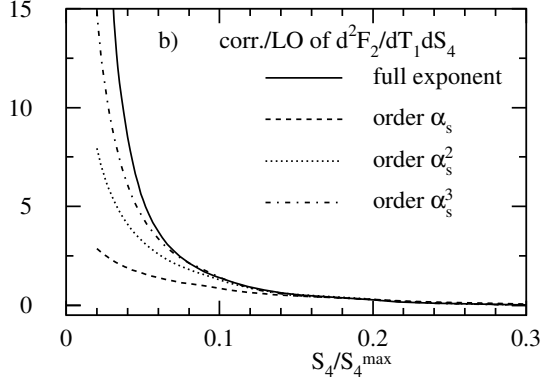


Fig. 5: Expandability of the resummed expressions for $d^2 F_2^c / dT_1 dS_4$ with NLL exponent (ratio to LO)

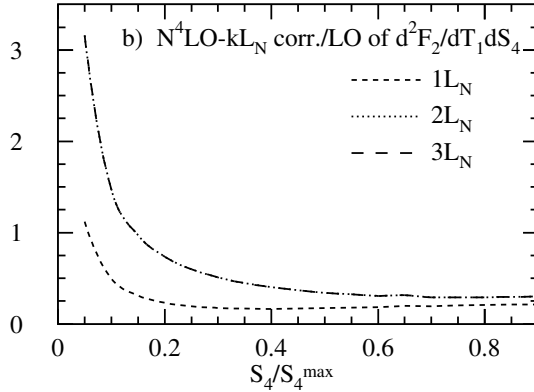


Fig. 6: Tower resummation at $N^4 \text{LO} - k L_N$, $k \in \{1, 2, 3\}$ ($N^4 \text{LO} - 2L_N$ and $N^4 \text{LO} - 3L_N$ almost coincide).

In Fig. 5 we evaluate this expansion as a function of the recoil mass S_4 , and compare it to its finite order expansions. We keep the variable T_1 fixed at the average of its minimum and maximum allowed value. Clearly, for reasonable values of S_4 the resummed result is already well-approximated by its 2nd and 3rd order expansions.

Another way to evaluate the resummed expression is in terms of towers of [78] $L = \ln N$.

$$\omega = h_{00}(\alpha_s) \left[1 + \sum_{k=1}^{\infty} \left(\frac{\alpha_s}{\pi} \right)^k \left(c_{k1} L^{2k} + c_{k2} L^{2k-1} + c_{k3} L^{2k-2} + \dots \right) \right]. \quad (26)$$

where the indicated coefficients c_{kj} can be determined exactly. More accuracy here means including more subleading towers. This method is equivalent, but not identical to the minimal prescription method. In practice, one need only include the first 4 terms in each tower, the higher terms are vanishingly small. The ambiguities mentioned earlier are shifted to far-subleading towers in this approach. To exhibit the convergence of terms in the towers, it will be useful and illustrative to exhibit contributions of a particular order in the strong coupling and the large logarithms. We will employ the notation

$$N^k \text{LO} - l L_N \quad (27)$$

for finite order results, where k indicates the order in the strong coupling, the subscript N denotes moments, and l expresses if only the leading term ($l = 1, L^{2k}$), or also the next-to-leading term ($l = 2, L^{2k-1}$) is included, etc. In Fig. 6 we see also in this approach a rapid convergence toward the tower-resummed result.

A more complete study of the relevance of threshold resummation for electroproduction of heavy quarks at HERA still awaits. We note that even if the size of the corrections does not cause much concern

for the perturbative analysis of an observable, threshold resummation or its finite order approximations, often lead to a reduction of scale dependence [79], indeed also seen in Ref. [76].

6 k_t - factorization⁷

6.1 Introduction

The transverse momenta of the partons initiating a hard scattering process, like heavy quark production via $\gamma g \rightarrow Q\bar{Q}$ or $gg \rightarrow Q\bar{Q}$ in lepto- (hadro-) production, respectively, is mainly generated by the QCD evolution, which can reach large values, in DGLAP up to the factorization scale, in BFKL/CCFM/LDC even larger.

The typical transverse momenta of the gluons in a process $gg \rightarrow X$ for different masses M of the system X are shown in Fig. 7 as a function of the momentum fraction x of one of the gluons for LHC energies. The transverse momenta can become large, so that they cannot be neglected. A

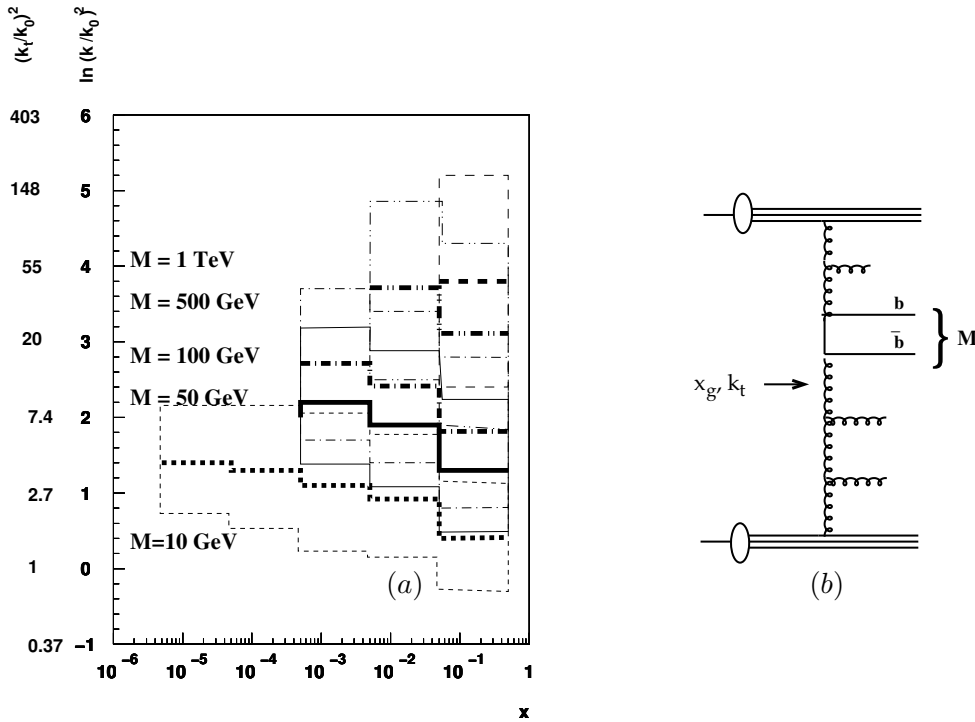


Fig. 7: Average transverse gluon momenta k_t in processes $gg \rightarrow X$ for different masses M of the system X as a function of the momentum fraction of one of the gluons x . The thin lines indicate the RMS spread of the distributions. In (b) is shown the definition of x , k_t and M for a gluon induced process.

theoretical approach, formulated for small x , which takes into account the transverse momenta is the k_t -factorization [80, 81] or semi-hard [82] approach.

In k_t -factorization the cross section for any process $pp \rightarrow X$ can be written as:

$$\sigma = \int dx_1 dx_2 \int dk_{t1} dk_{t2} \mathcal{A}(x_1, k_{t1}, q) \mathcal{A}(x_2, k_{t2}, q) \hat{\sigma}(x_1, x_2, k_{t1} k_{t2}, q) \quad (28)$$

with $\mathcal{A}(x, k_t, q)$ being the un-integrated (k_t -dependent) parton density function uPDF, q defines the factorization scale and $\hat{\sigma}$ is the partonic cross section. The off-shell matrix-elements $\hat{\sigma}$ are calculated in [80, 81].

⁷Contributed by S.P. Baranov, H. Jung, A.V. Lipatov and N.P. Zotov

The effects of finite transverse momenta are present independent of the evolution scheme: uPDFs can be defined also for the DGLAP evolution. A more detailed discussion on these effects can be found in [83, 84].

It is interesting to note, that the k_t -factorization approach (in LO α_s) agrees very well with calculations performed in the collinear approach in NLO α_s , which is shown in [85]. The main effect comes from a more realistic treatment of the kinematics already in LO, which otherwise has to be covered in NLO. The k_t factorization approach, however, is strictly valid only at small x , where the virtuality of the exchanged gluons can be identified with its transverse momentum $k^2 \sim -k_t^2$. The full expression for the virtuality is [86]:

$$k^2 = \frac{-k_t^2}{1-x} - \frac{x \cdot m^2}{1-x} \quad (29)$$

with m being the recoiling mass of the hadronic system except the hard scattering process, taking into account the history of the evolution process. For finite x the mass effects can be substantial.

6.2 Open $b\bar{b}$ production and correlations at the LHC

Heavy quark production in the k_t -factorization approach at HERA and the Tevatron was considered already in many papers (see, for example, [82, 87–90]). In Ref. [91] the k_t -factorization approach was used for a more detailed analysis of the D0 and CDF experimental data. The effect of the initial gluon transverse momenta on the kinematics of the $b\bar{b}$ production at the LHC were investigated [92]. The renormalization and factorization scales were set equal to either the initial gluon virtualities, $\mu_R^2 = \mu_F^2 = q_{T1,2}^2$, or $\mu_F^2 = m_{bT}^2$, as is in the standard collinear QCD, and the quark mass of $m_b = 4.75$ GeV was used.

In Fig. 8a we show the transverse momentum distributions of B mesons at LHC energies. The calculation was performed in the range $|\eta^B| < 1$ and the Peterson fragmentation with $\epsilon = 0.006$ using the KMS [93] parameterization for the un-integrated gluon density (see [83, 84]). The prediction for the azimuthal correlations between the muons coming from B meson decays are shown in Fig. 8b with $p_t^\mu > 6$ GeV and $|\eta^\mu| < 2.5$. The azimuthal correlations indicate an important theoretical difference

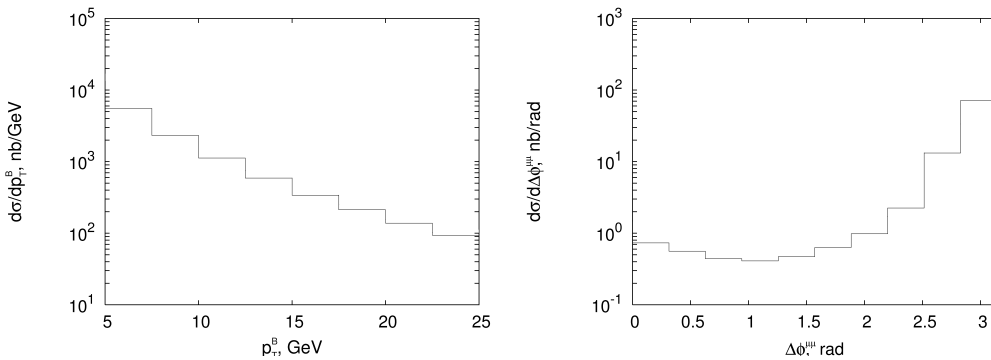


Fig. 8: Prediction for B -meson production at the LHC using the KMS un-integrated gluon density. In *a* the p_T distribution of B -mesons is shown. In *b* the azimuthal $\mu\mu$ correlation coming from the B decays is shown.

between the collinear and k_t -factorization approaches. In the collinear approximation at parton level and leading order, the b quarks are produced exactly back-to-back, which is clearly unphysical when the gluon is evolved up to a large enough scale. Only starting with NLO a significant deviation from the back-to-back scenario is found. Thus the NLO calculation has to correct for the wrong kinematics in LO together with higher order corrections, leading to large K factors. In the k_t -factorization, the transverse momenta of the gluons are correctly treated already in LO. In the k_t -factorization approach the NLO corrections are therefore expected to be much smaller, since here only the purely dynamical corrections have to be applied, whereas the kinematics are already correctly treated in LO.

6.3 Quarkonium production and polarization at the LHC

Since the initial gluons have non-zero transverse momenta, they are off-shell, and they have a longitudinal component in their polarization vector. Typically, the k_t values of the two colliding gluons are much different, as the parton evolution is equivalent to the random walk in the $\ln |k_t|$ plane, not in k_t plane. Roughly speaking, the k_t of one of the gluons can be neglected in comparison with that of the other. So, in the initial state we have one nearly on-shell (transversely polarized) gluon and one off-shell (longitudinally polarized) gluon. After the interaction, they convert into one on-shell gluon and a heavy vector meson. Simple helicity conservation arguments show that the polarization of vector meson must be longitudinal, in contrast with the ordinary parton model, where the initial gluons are both on-shell. This effect has been already studied for the HERA [94] and Tevatron [95] conditions. Fig.9a shows the predictions for the LHC energy obtained with KMS [93] parameterization for un-integrated gluon densities. The calculations are restricted to the pseudorapidity interval $-2.5 < \eta_\Upsilon < 2.5$ and assume ATLAS "μ6μ3" trigger cut, which means one muon with $p_t > 6$ GeV and another muon with $p_t > 3$ GeV.

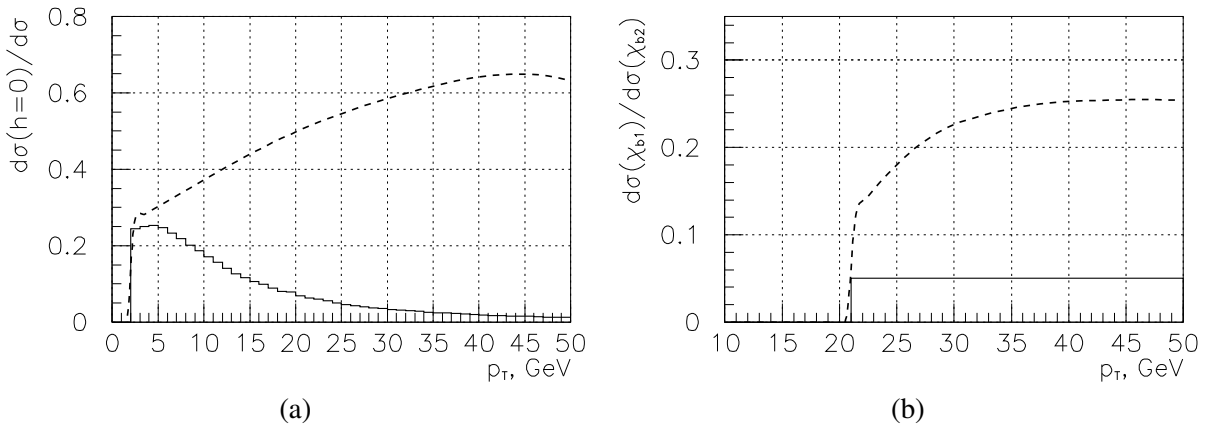


Fig. 9: Predictions of different theoretical approaches for quarkonium production. In (a) the fraction of longitudinally polarized Υ mesons is shown: solid histogram – collinear parton model, singlet + octet; dashed – k_t -factorization with KMS u.g.d.. In (b) the ratio of the production rates χ_{b1}/χ_{b2} is shown: solid histogram – collinear parton model, singlet + octet; dashed – k_t factorization with KMS u.g.d.

Important effects are also seen in the production of P -wave bottomium states with different spins χ_{b1} and χ_{b2} . At the Tevatron energies, this process has been considered in Ref. [96], and the predictions for the LHC are presented in Fig.9b. The P -wave states are assumed to be detected via the decay $\chi_b \rightarrow \Upsilon + \gamma$, with an additional requirement that the energy of the decay photon be greater than 2 GeV. The ratio of the production rates $\sigma(\chi_1)/\sigma(\chi_2)$ is qualitatively different in the k_t -factorization and the collinear parton model. The underlying physics is clearly connected with gluon off-shellness. In the collinear parton model, the relative suppression of χ_1 states becomes stronger with increasing p_T because of the increasing role of the color-octet contribution: in this approach, the leading-order fragmentation of an on-shell transversely polarized gluon into a vector meson is forbidden. In contrast with that, in the k_t -factorization approach, the increase in the final state p_T is only due to the increasing transverse momenta (and virtualities) of the initial gluons, and, consequently, the suppression motivated by the Landau-Yang theorem becomes weaker at large p_T .

6.4 Associated Higgs + jets production at the LHC

The dominant mechanism for Higgs production at the LHC is gluon-gluon fusion, and the calculations can be significantly simplified in the large top mass limit ($M_H \leq 2M_{top}$) [97].

The differential cross section of the inclusive Higgs production $p\bar{p} \rightarrow H + X$ in the k_t -factorization approach has been calculated in [98,99] and can be written as:

$$\frac{d\sigma(p\bar{p} \rightarrow H + X)}{dy_H} = \int \frac{\alpha_s^2(\mu^2)}{288\pi} \frac{G_F\sqrt{2}}{x_1x_2m_H^2s} [m_H^2 + \mathbf{p}_T^2]^2 \cos^2(\Delta\varphi) \times \mathcal{A}(x_1, \mathbf{k}_{1T}^2, \mu^2) \mathcal{A}(x_2, \mathbf{k}_{2T}^2, \mu^2) d\mathbf{k}_{1T}^2 d\mathbf{k}_{2T}^2 \frac{d(\Delta\varphi)}{2\pi}, \quad (30)$$

where G_F is the Fermi coupling constant, $\mathcal{A}(x, \mathbf{k}_T^2, \mu^2)$ is the un-integrated gluon distribution, $\Delta\varphi$ the azimuthal angle between the momenta \mathbf{k}_{1T} and \mathbf{k}_{2T} , and the transverse momentum of the produced Higgs boson is $\mathbf{p}_T = \mathbf{k}_{1T} + \mathbf{k}_{2T}$. It should be noted, that this process is particularly interesting in k_t -factorization, as the transverse momenta of the gluons are in the same order as their longitudinal momenta ($\sim \mathcal{O}(10 \text{ GeV})$) [100].

The total inclusive Higgs production cross section at the LHC energies ($\sqrt{s} = 14 \text{ TeV}$) is plotted in Fig. 10(a) as a function of the Higgs mass in the mass range $m_H = 100 - 200 \text{ GeV}$. The solid line is obtained by fixing both the factorization and renormalization scales at the default value $\mu = m_H$ with the J2003 (set 1) CCFM un-integrated gluon distribution [101]. In order to estimate the theoretical uncertainties, we take $\mu = \xi m_H$ and vary the scale parameter ξ between 1/2 and 2 about the default value $\xi = 1$. The uncertainty band is presented by the upper and lower dashed lines. We find that our central values agree very well with recent NNLO results [102].

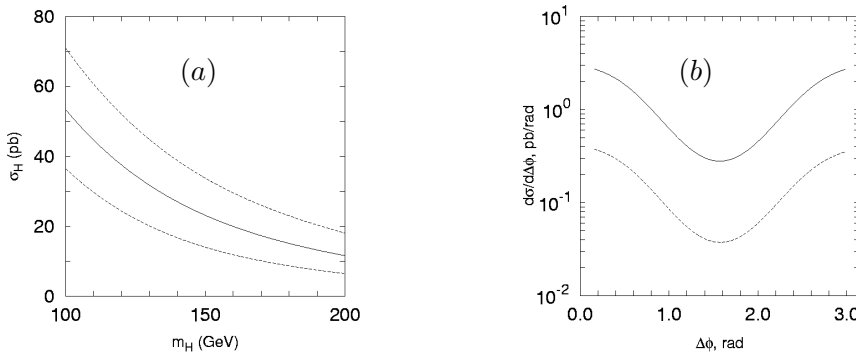


Fig. 10: Higgs production at the LHC. In (a) the total cross section for Higgs boson production as a function of Higgs mass is shown: the solid curve corresponds to the default scale $\mu = m_H$, upper and lower dashed curves - $\mu = m_H/2$ and $\mu = 2m_H/2$ respectively. In (b) the jet-jet azimuthal angle distribution in the Higgs+jet+jet production at $\sqrt{s} = 14 \text{ TeV}$. The kinematical cut $|\mathbf{p}_{\text{jet } T}| > 20 \text{ GeV}$ was applied for both jets. Solid and dashed lines correspond to the J2003 (set 1) and J2003 (set 2) [101] u.g.d. respectively.

To demonstrate the capabilities of the k_t -factorization approach, we calculate the azimuthal angle $\Delta\phi$ distribution between the two final jets transverse momenta in the Higgs+jet+jet production process. Our results are shown in Fig. 10(b). The dip at $\Delta\phi = \pi/2$ comes from the $\cos(\Delta\varphi)$ in eq.(30). In the approach presented here, the k_t of the initial gluons is approximately compensated by the transverse momenta of the jets [103]: $\mathbf{k}_T \simeq -\mathbf{p}_{T,\text{jet}}$, and, consequently, $\Delta\phi \simeq \Delta\varphi$ applying a cut-off $|\mathbf{p}_{\text{jet } T}| > 20 \text{ GeV}$. This dip is characteristic for the loop-induced Higgs coupling to gluons in the framework of fixed-order perturbative QCD calculations [102]. Thus, we illustrate that the features usually interpreted as NNLO effects are reproduced in the k_t -factorization with LO matrix elements.

However, we see a very large difference (about one order of magnitude) between the predictions based on the J2003 gluon densities set 1 and set 2 [101], showing the sensitivity to the shape of the un-integrated gluon density.

6.5 Conclusions

The finite k_t of the initial state gluons significantly modifies the kinematics of the gluon-gluon fusion process and leads to nontrivial angular correlations between the final state heavy quarks. The longitudinal polarization of the initial off-shell gluons manifests in the longitudinal polarization of J/ψ and Υ mesons at moderate p_T and, also, affects the production rates of P -wave quarkonia.

The predictions in k_t -factorization are very close to NNLO pQCD results for the inclusive Higgs production at the LHC, since the main part of high-order collinear pQCD corrections is already included in the k_t -factorization. In the k_t -factorization approach the calculation of associated Higgs+jets production is much simpler than in the collinear factorization approach. However, the large scale dependence of our calculations (of the order of 20 – 50%) probably indicates the sensitivity to the unintegrated gluon distributions.

7 Baryon charge transfer and production asymmetry of $\Lambda^0/\bar{\Lambda}^0$ in hadron interactions⁸

7.1 Introduction to the QGSM

The phenomenon of nonzero asymmetry of baryon production with nonbaryonic beams (π, μ, e) was mentioned and explained in a few theoretical papers. Baryon charge can be transferred from proton or nucleus targets through the large rapidity gap with the string junction. In baryonic beam reactions (p, A , etc.) this effect is displayed in the valuable baryon/antibaryon spectrum asymmetry at $y = 0$. Every theoretical discourse on baryon charge transfer appeals to the value of the intercept, $\alpha_{S,J}(0)$, that is an intercept of the Regge-trajectory of imaginary particles which consists only of string junctions from baryon and antibaryon. Practically, the models that can account for this effect are only non perturbative QCD phenomenological models: the Dual Parton Model (DPM) [104] and the Quark Gluon String Model (QGSM) [105] as well as the DPMJET Monte Carlo expansion of these two models. Both analytical models are similar and they were based on the common Regge asymptotic presentation of constituent quark structure functions and string (quark) fragmentation functions. Here we are considering QGSM. In the comparison to the other models, QGSM accounts for many Pomeron exchanges. This approach works very well to give us the correct description of particle production cross sections at very high energies. The QGSM procedures of constructing of quark/diquark structure functions and fragmentation functions were presented in many previous publications. We take into consideration the π - p reaction that gives similar asymmetries as the γ - p reaction. The spectra in this reaction are more sensitive to the baryon excess in the region of positive x_F than the spectra of baryons in p - p collisions.

7.2 Comparison with Experimental Data

The asymmetry $A(y)$ between the spectra of baryons and antibaryons is defined as:

$$A(x) = \frac{dN^{\Lambda^0}/dx - dN^{\bar{\Lambda}^0}/dx}{dN^{\Lambda^0}/dx + dN^{\bar{\Lambda}^0}/dx}, \quad (31)$$

The EHS and the NA49 experiments have presented evidence for a nonzero baryon production asymmetry in proton-proton fixed target interactions, measuring at $y = 0$ values of the order of 0.5 - 0.3. In pion-proton interactions (E769) we can see the y dependence of the asymmetry and the measured asymmetry, which was multiplied by a factor of 2 in order to be compared with the pp asymmetry.

The data from these experiments can be presented in one plot for $A(\Delta y)$, where Δy is the rapidity distance from interacting target-proton (see Fig. 11). It is seen that the points are situated on the same line. If we add the data from proton-nucleus experiments (HERA-B and RHIC) they are still approximately on this line. Only the STAR asymmetry point at $\sqrt{s} = 130$ GeV can be interpreted as a sign that the curve is bent. And the result of the H1 experiment at HERA [106] calls certainly for a steeper curve.

⁸Contributed by O.I. Piskounova.

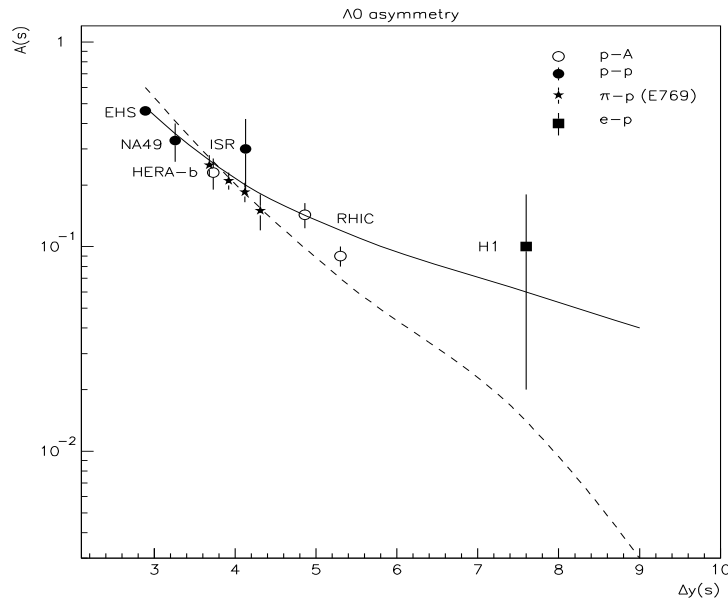


Fig. 11: Asymmetry in Λ^0 and $\bar{\Lambda}^0$ production and QGSM curves: $\alpha_{SJ}(0)=0.5$ (dashed line) and $\alpha_{SJ}(0)=0.9$ (solid line).

What means do we have in QGSM to describe this dependence? In Ref. [107] it was shown that the data of the E769 and H1 experiments can not be described with the same value of $\alpha_{SJ}(0)$: the points at lower energy correspond to $\alpha_{SJ}(0)=0.5$, while the H1 point requires $\alpha_{SJ}(0)=0.9$.

7.3 Summary

The purpose of this contribution is to show the band of asymmetries that can be predicted for the LHC experiments between the two possibilities given above for $\alpha_{SJ}(0)$. The results are shown in Fig. 11. The solid line represents the case of $\alpha_{SJ}(0)=0.9$. This curve fits the data at low energies (small Δy) due to varying the energy splitting between string junction and diquark configuration: $0.1 \cdot \text{SJ} + 0.9 \cdot \text{DQ}$. What we had to tune also was the fragmentation parameter $af=0.15$ instead of 0.2 accepted in previous papers. Also the curve for $\alpha_{SJ}(0)=0.5$ is shown in Fig. 11 with a dashed line. This line certainly doesn't fit the H1 point and gives a negligible asymmetry at the energy of the LHC experiments. Finally, we have the prediction for strange baryon asymmetries at the LHC within the range: $0.003 < A < 0.04$. The same procedure has to be applied to charmed baryon asymmetry to get the predictions at LHC energy.

References

- [1] W. Stirling. Private communication
- [2] P. Nason, S. Dawson, and R. K. Ellis, Nucl. Phys. **B303**, 607 (1988)
- [3] W. Beenakker, H. Kuijf, W. L. van Neerven, and J. Smith, Phys. Rev. **D40**, 54 (1989)
- [4] P. Nason, S. Dawson, and R. K. Ellis, Nucl. Phys. **B327**, 49 (1989). Erratum-ibid. B **335** (1989) 260
- [5] W. Beenakker, W. L. van Neerven, R. Meng, G. A. Schuler, and J. Smith, Nucl. Phys. **B351**, 507 (1991)
- [6] M. L. Mangano, P. Nason, and G. Ridolfi, Nucl. Phys. **B373**, 295 (1992)
- [7] R. K. Ellis and P. Nason, Nucl. Phys. **B312**, 551 (1989)
- [8] J. Smith and W. L. van Neerven, Nucl. Phys. **B374**, 36 (1992)

- [9] S. Frixione, M. L. Mangano, P. Nason, and G. Ridolfi, Nucl. Phys. **B412**, 225 (1994).
hep-ph/9306337
- [10] E. Laenen, S. Riemersma, J. Smith, and W. L. van Neerven, Nucl. Phys. **B392**, 162 (1993)
- [11] E. Laenen, S. Riemersma, J. Smith, and W. L. van Neerven, Nucl. Phys. **B392**, 229 (1993)
- [12] S. Riemersma, J. Smith, and W. L. van Neerven, Phys. Lett. **B347**, 143 (1995).
hep-ph/9411431
- [13] B. W. Harris and J. Smith, Nucl. Phys. **B452**, 109 (1995). hep-ph/9503484
- [14] J. C. Collins and W.-K. Tung, Nucl. Phys. **B278**, 934 (1986)
- [15] B. Mele and P. Nason, Nucl. Phys. **B361**, 626 (1991)
- [16] M. A. G. Aivazis, F. I. Olness, and W.-K. Tung, Phys. Rev. **D50**, 3085 (1994). hep-ph/9312318
- [17] M. A. G. Aivazis, J. C. Collins, F. I. Olness, and W.-K. Tung, Phys. Rev. **D50**, 3102 (1994).
hep-ph/9312319
- [18] J. C. Collins, Phys. Rev. **D58**, 094002 (1998). hep-ph/9806259
- [19] M. Kramer, F. I. Olness, and D. E. Soper, Phys. Rev. **D62**, 096007 (2000). hep-ph/0003035
- [20] J. C. Collins, F. Wilczek, and A. Zee, Phys. Rev. **D18**, 242 (1978)
- [21] W.-K. Tung, S. Kretzer, and C. Schmidt, J. Phys. **G28**, 983 (2002). hep-ph/0110247
- [22] S. Kretzer, H. L. Lai, F. I. Olness, and W. K. Tung, Phys. Rev. **D69**, 114005 (2004).
hep-ph/0307022
- [23] S. Kretzer and F. I. Olness (2005). hep-ph/0508216
- [24] M. Cacciari, M. Greco, and P. Nason, JHEP **05**, 007 (1998). hep-ph/9803400
- [25] R. S. Thorne and R. G. Roberts, Phys. Rev. **D57**, 6871 (1998). hep-ph/9709442
- [26] R. S. Thorne and R. G. Roberts, Phys. Lett. **B421**, 303 (1998). hep-ph/9711223
- [27] A. Chuvakin, J. Smith, and W. L. van Neerven, Phys. Rev. **D61**, 096004 (2000).
hep-ph/9910250
- [28] M. Gluck, E. Reya, and M. Stratmann, Nucl. Phys. **B422**, 37 (1994)
- [29] M. Buza, Y. Matiounine, J. Smith, R. Migneron, and W. L. van Neerven, Nucl. Phys.
B472, 611 (1996). hep-ph/9601302
- [30] M. Buza, Y. Matiounine, J. Smith, and W. L. van Neerven, Phys. Lett. **B411**, 211 (1997).
hep-ph/9707263
- [31] M. Buza, Y. Matiounine, J. Smith, and W. L. van Neerven, Eur. Phys. J. **C1**, 301 (1998).
hep-ph/9612398
- [32] Y. Matiounine, J. Smith, and W. L. van Neerven, Phys. Rev. **D57**, 6701 (1998).
hep-ph/9801224
- [33] A. Chuvakin, J. Smith, and W. L. van Neerven, Phys. Rev. **D62**, 036004 (2000).
hep-ph/0002011
- [34] A. Chuvakin and J. Smith, Comput. Phys. Commun. **143**, 257 (2002). hep-ph/0103177
- [35] A. Vogt, Comput. Phys. Commun. **170**, 65 (2005). hep-ph/0408244
- [36] A. Chuvakin, J. Smith, and B. W. Harris, Eur. Phys. J. **C18**, 547 (2001). hep-ph/0010350
- [37] M. Cacciari and M. Greco, Nucl. Phys. **B421**, 530 (1994). hep-ph/9311260
- [38] M. Cacciari and M. Greco, Z. Phys. **C69**, 459 (1996). hep-ph/9505419
- [39] M. Cacciari, S. Frixione, and P. Nason, JHEP **03**, 006 (2001). hep-ph/0102134
- [40] F. Aversa, P. Chiappetta, M. Greco, and J. P. Guillet, Nucl. Phys. **B327**, 105 (1989)
- [41] S. Frixione and P. Nason, JHEP **03**, 053 (2002). hep-ph/0201281
- [42] M. Cacciari and P. Nason, Phys. Rev. Lett. **89**, 122003 (2002). hep-ph/0204025
- [43] M. Cacciari and P. Nason, JHEP **09**, 006 (2003). hep-ph/0306212

- [44] M. Cacciari, S. Frixione, M. L. Mangano, P. Nason, and G. Ridolfi, *JHEP* **07**, 033 (2004). [hep-ph/0312132](#)
- [45] M. Cacciari, P. Nason, and R. Vogt, *Phys. Rev. Lett.* **95**, 122001 (2005). [hep-ph/0502203](#)
- [46] B. A. Kniehl, G. Kramer, I. Schienbein, and H. Spiesberger, *Phys. Rev.* **D71**, 014018 (2005). [hep-ph/0410289](#)
- [47] B. A. Kniehl, G. Kramer, I. Schienbein, and H. Spiesberger, *Eur. Phys. J.* **C41**, 199 (2005). [hep-ph/0502194](#)
- [48] F. I. Olness, R. J. Scalise, and W.-K. Tung, *Phys. Rev.* **D59**, 014506 (1999). [hep-ph/9712494](#)
- [49] B. A. Kniehl, T. Kneesch, G. Kramer, and I. Schienbein, work in progress
- [50] S. Kretzer and I. Schienbein, *Phys. Rev.* **D58**, 094035 (1998). [hep-ph/9805233](#)
- [51] S. Kretzer and I. Schienbein, *Phys. Rev.* **D59**, 054004 (1999). [hep-ph/9808375](#)
- [52] G. Kramer and H. Spiesberger, *Eur. Phys. J.* **C22**, 289 (2001). [hep-ph/0109167](#)
- [53] G. Kramer and H. Spiesberger, *Eur. Phys. J.* **C28**, 495 (2003). [hep-ph/0302081](#)
- [54] G. Kramer and H. Spiesberger, *Eur. Phys. J.* **C38**, 309 (2004). [hep-ph/0311062](#)
- [55] J. Pumplin *et al.*, *JHEP* **07**, 012 (2002). [hep-ph/0201195](#)
- [56] B. A. Kniehl, G. Kramer, I. Schienbein, and H. Spiesberger, in preparation
- [57] CDF Collaboration, D. Acosta *et al.*, *Phys. Rev. Lett.* **91**, 241804 (2003). [hep-ex/0307080](#)
- [58] B. A. Kniehl, G. Kramer, I. Schienbein, and H. Spiesberger, *Hadroproduction of d and b mesons in a massive vfn*s, 2005. Proceedings of the 13th International Workshop on Deep Inelastic Scattering (DIS 2005), Madison, Wisconsin, USA, April 27 - May 1, 2005., [hep-ph/0507068](#)
- [59] B. A. Kniehl, G. Kramer, I. Schienbein, and H. Spiesberger, *Reconciling open charm production at the fermilab tevatron with qcd*, 2005. [hep-ph/0508129](#)
- [60] J. Binnewies, B. A. Kniehl, and G. Kramer, *Phys. Rev.* **D58**, 014014 (1998). [hep-ph/9712482](#)
- [61] CDF Collaboration, D. Acosta *et al.*, *Phys. Rev.* **D71**, 012005 (2005). [hep-ex/0410058](#)
- [62] D0 Collaboration, V. M. Abazov *et al.*, *Phys. Lett.* **B622**, 265 (2005). [hep-ex/0505063](#)
- [63] J. Campbell *et al.*, *Higgs boson production in association with bottom quarks* (unpublished). 2004
- [64] H1 Collaboration, A. Aktas *et al.*, *Eur. Phys. J.* **C40**, 349 (2005). [hep-ex/0411046](#)
- [65] H1 Collaboration, A. Aktas *et al.* (2005). [hep-ex/0507081](#)
- [66] M. Dittmar and K. Mazumdar, *Measuring the parton Distribution functions of charm, beauty and strange quarks and anti-quarks at the LHC* (unpublished). CMS note 2001/002
- [67] J. Campbell, R. K. Ellis, F. Maltoni, and S. Willenbrock, *Phys. Rev.* **D69**, 074021 (2004). [hep-ph/0312024](#)
- [68] D0 Collaboration, V. M. Abazov *et al.*, *Phys. Rev. Lett.* **94**, 161801 (2005). [hep-ex/0410078](#)
- [69] C. Kao and N. Stepanov, *Phys. Rev.* **D52**, 5025 (1995). [hep-ph/9503415](#)
- [70] V. D. Barger and C. Kao, *Phys. Lett.* **B424**, 69 (1998). [hep-ph/9711328](#)
- [71] S. Dawson, D. Dicus, and C. Kao, *Phys. Lett.* **B545**, 132 (2002). [hep-ph/0208063](#)
- [72] T. Sjostrand *et al.*, *Comput. Phys. Commun.* **135**, 238 (2001). [hep-ph/0010017](#)
- [73] E. Richter-Was, *AtlfastTemp package- ATLAS fast simulation (fortran) integrated with Athena framework* (unpublished). ATLAS internal note ATL-COM-PHYS-2000-023
- [74] G. Serman, *Nucl. Phys.* **B281**, 310 (1987)
- [75] S. Catani and L. Trentadue, *Nucl. Phys.* **B327**, 323 (1989)
- [76] E. Laenen and S.-O. Moch, *Phys. Rev.* **D59**, 034027 (1999). [hep-ph/9809550](#)
- [77] S. Catani, M. L. Mangano, P. Nason, and L. Trentadue, *Nucl. Phys.* **B478**, 273 (1996). [hep-ph/9604351](#)

- [78] A. Vogt, Phys. Lett. **B471**, 97 (1999). hep-ph/9910545
- [79] G. Sterman and W. Vogelsang, hep-ph/0002132 (2000). hep-ph/0002132
- [80] S. Catani, M. Ciafaloni, and F. Hautmann, Nucl. Phys. **B 366**, 135 (1991)
- [81] J. Collins and R. Ellis, Nucl. Phys. **B 360**, 3 (1991)
- [82] E. Levin, M. Ryskin, Y. Shabelski, and A. Shuvaev, Sov. J. Nucl. Phys. **53**, 657 (1991)
- [83] Small x Collaboration, B. A. et al., Eur. Phys. J. **C 25**, 77 (2002). hep-ph/0204115
- [84] Small x Collaboration, J. R. Andersen *et al.*, Eur. Phys. J. **C35**, 67 (2004). hep-ph/0312333
- [85] M. C. et al, *Benchmark cross sections for heavy flavor production*, 2005. This proceedings
- [86] J. Collins and H. Jung, *Need for fully unintegrated parton densities*, 2005. hep-ph/0508280 and these proceedings
- [87] M. Ryskin, A. Shuvaev, and Y. Shabelski, Phys. Atom. Nucl. **64**, 120 (2001). hep-ph/9907507
- [88] P. Hagler, R. Kirschner, A. Schafer, L. Szymanowski, and O. Teryaev, Phys. Rev. **D62**, 071502 (2000). hep-ph/0002077
- [89] A. V. Lipatov, L. Lonnblad, and N. P. Zotov, JHEP **01**, 010 (2004). hep-ph/0309207
- [90] H. Jung, Phys. Rev. **D 65**, 034015 (2002). DESY-01-136, hep-ph/0110034
- [91] S. P. Baranov, N. P. Zotov, and A. V. Lipatov, Phys. Atom. Nucl. **67**, 837 (2004)
- [92] S. P. Baranov, A. V. Lipatov, and N. P. Zotov, Nucl. Phys. Proc. Suppl. **146**, 228 (2005)
- [93] J. Kwiecinski, A. Martin, and A. Stasto, Phys. Rev. **D 56**, 3991 (1997)
- [94] A. V. Lipatov and N. P. Zotov, Eur. Phys. J. **C27**, 87 (2003). hep-ph/0210310S. P. Baranov and N. P. Zotov, J. Phys. **G29**, 1395 (2003). hep-ph/0302022
- [95] S. P. Baranov, Phys. Rev. **D66**, 114003 (2002)
- [96] S. P. Baranov, Phys. Lett. **B594**, 277 (2004)
- [97] J. Ellis, M. Gaillard, and D. Nanopoulos, Nucl. Phys. **B106**, 292 (1976)M. A. Shifman, A. I. Vainshtein, M. B. Voloshin, and V. I. Zakharov, Sov. J. Nucl. Phys. **30**, 711 (1979)
- [98] F. Hautmann, Phys. Lett. **B535**, 159 (2002). hep-ph/0203140
- [99] A. V. Lipatov and N. P. Zotov, *Higgs boson production at hadron colliders in the $k(t)$ -factorization approach*, 2005. hep-ph/0501172, DESY-05-020
- [100] H. Jung, Mod. Phys. Lett. **A19**, 1 (2004). hep-ph/0311249
- [101] M. Hansson and H. Jung, *The status of ccfm unintegrated gluon densities*, 23-27 April 2003. DIS 2003, St. Petersburg, Russia, hep-ph/0309009
- [102] R. Harlander and W. Kilgore, Phys. Rev. Lett. **88**, 201801 (2002). hep-ph/0201206C. Anastasiou and K. Melnikov, Nucl. Phys. **B646**, 220 (2002). hep-ph/0207004V. Ravindran, J. Smith, and W. van Neerven, Nucl. Phys. **B665**, 325 (2003). hep-ph/0302135
- [103] S. P. Baranov. and N. P. Zotov, Phys. Lett. **B491**, 111 (2000)
- [104] A. Capella and J. Tran Thanh Van, Z. Phys. **C10**, 249 (1981)
- [105] A. B. Kaidalov and K. A. Ter-Martirosian, Sov. J. Nucl. Phys. **39**, 979 (1984)
- [106] H1 Collaboration, C. Adloff *et al.*, Z. Phys. **C76**, 613 (1997). hep-ex/9708016
- [107] G. H. Arakelian, A. Capella, A. B. Kaidalov, and Y. M. Shabelski, Eur. Phys. J. **C26**, 81 (2002)